Deep Alternating Projection Networks for Gridless DOA Estimation With Nested Array

Xiaolong Su, Panhe Hu, Zhen Liu, Junpeng Shi, and Xiang Li

***Abstract*—Recently, deep unfolding networks with interpretable parameters have been widely utilized in direction of arrival (DOA) estimation due to the faster convergence speed and better generalization ability. However, few consider the nested array for gridless DOA estimation. In this letter, we propose a deep alternating projection network to address the problem. We first convert the covariance matrix into a measurement vector in the form of atomic norm, which can reduce the matrix dimension during projection. We then train the proposed network to alternately obtain the positive semi-definite matrix and the corresponding irregular Hermitian Toeplitz matrix, where the loss function is derived by employing the trace of network output. Finally, we apply the irregular root Multiple Signal Classification (MUSIC) method to obtain gridless DOA via nested array. We demonstrate that the proposed networks can accelerate the convergence rate and reduce computational cost. Simulations verify the performance of proposed networks in comparison with the existing methods.**

***Index Terms*—Gridless, direction of arrival (DOA), deep unfolding network, alternating projection, nested array.**

I. Introduction

DIRECTION of arrival (DOA) estimation plays an important role in phased array radar, passive sonar and wireless communications [1]–[4]. Previous grid-based methods consider the estimated DOAs selected from finite grid points. However, the performance of DOA estimation suffers from the problem of grid mismatch. Recently, the state of the art researches have exploited off-grid [5]–[6] or gridless methods [7]–[10] to achieve DOA estimation. In [7], the deterministic atomic norm optimization is applied to obtain gridless DOA estimation in the case of limited snapshots, where the constraint is related to the covariance matrix. In order to overcome the high computational cost of interpolation methods, the alternating projection method in [9] is proposed to achieve gridless DOA estimation with a certain number of iterations. Moreover, by applying the geometry of sparse linear array, the dual formulation of atomic norm minimization method in [10] is utilized to improve the accuracy of gridless DOA estimation. Compared with the uniform linear arrays, the sparse linear arrays (e.g., nested array and coprime array) require fewer sensors with the same aperture, which can reduce hardware costs [11]–[13]. Noticeably, the deep unfolding networks have been proposed to address the sparse recovery problem [14], which has the advantages of both model-driven methods and data-driven methods [15]–[17]. By transforming the iterative steps into the hidden layers with interpretable parameters, the Projected Gradient Descent (PGD) algorithm in [18] is unrolled in the network with the fully connected layers between non-adjacent layers, which can enhance the performance of sparse reconstruction. Moreover, the ADMM-net is proposed in [19] for sparse aperture ISAR imaging, which can accelerate the convergence rate and reduce computational cost.

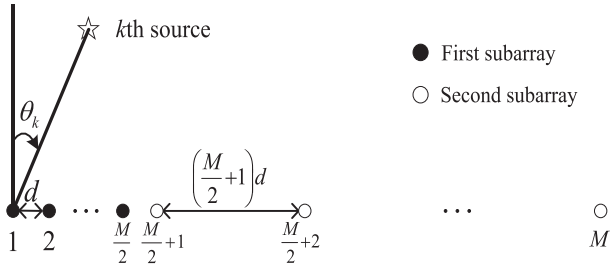

Fig. 1. Structure of two-level nested array.

Accordingly, the motivation of this work is to apply deep unfolding network with alternative projections for gridless DOA estimation with nested array. Firstly, the covariance matrix is transformed into a measurement vector in the form of atomic norm. Next, the deep alternating projection network is constructed to obtain the positive semi-definite matrix and the corresponding irregular Hermitian Toeplitz matrix to solve nonconvex optimization. Finally, the irregular root Multiple Signal Classification (MUSIC) method is utilized to obtain gridless DOA via nested array. Numerial simulation results demonstrate that the proposed deep alternating projection network can accelerate the convergence rate and reduce computational cost in comparison of the existing methods.

II. Signal Model With Nested Array

As depicted in Fig. 1, the sensors of two-level nested array are located at

$$\xi_m = \begin{cases} md, m = 1, 2, \ldots, M/2 \\ (m - M/2)(M/2 + 1)d, m \\ = M/2 + 1, M/2 + 2, \ldots, M. \end{cases} \quad (1)$$

Manuscript received 29 April 2022; revised 22 June 2022; accepted 29 June 2022. Date of publication 5 July 2022; date of current version 22 July 2022. This work was supported in part by National Key Research and Development Program of China under Grant 2021YFB3100800, in part by the National Natural Science Foundation of China under Grants 62022091, 62071476, and 61921001, in part by the Science and Technology Innovation Program of Hunan Province under Grants 2020RC2041 and 2021RC3079, and in part by the Research Program of National University of Defense Technology under Grants ZK20-33 and ZK21-14. The associate editor coordinating the review of this manuscript and approving it for publication was Prof. Jun Liu. *(Corresponding author: Panhe Hu.)*

The authors are with the College of Electronic Science and Technology, National University of Defense Technology, Changsha 410073, China (e-mail: suxiaolong_nudt@163.com; hupanhe13@nudt.edu.cn; zhen_liu@nudt.edu.cn; shijunpeng20@nudt.edu.cn; lixiang01@vip.sina.com).

Digital Object Identifier 10.1109/LSP.2022.3188446

1070-9908 © 2022 IEEE. Personal use is permitted, but republication/redistribution requires IEEE permission.
See https://www.ieee.org/publications/rights/index.html for more information.

Authorized licensed use limited to: Chang'an University. Downloaded on December 05,2022 at 14:08:01 UTC from IEEE Xplore. Restrictions apply.

Accordingly, the array output at the *n*th snapshot is given by

$$\begin{aligned}\mathbf{x}(n) &= \left[\, x_1(n)\ x_2(n)\ \cdots\ x_M(n) \,\right]^{\mathrm{T}} \\ &= \sum_{k=1}^{K} \mathbf{a}(\theta_k) s_k(n) + \mathbf{w}(n) \\ &= \mathbf{A}\mathbf{s}(n) + \mathbf{w}(n) \end{aligned} \tag{2}$$

where $(\bullet)^{\mathrm{T}}$ denotes transpose operator, $n = 12,\ldots,N$, $k = 12,\ldots, K$, N and K respectively denote snapshot number and source number, $\mathbf{s}(n) = [s_1(n)\ s_2(n)\ \cdots\ s_K(n)]^{\mathrm{T}}$ denotes the incoherent transmitted sources at the nth snapshot, $\mathbf{w}(n) = [w_1(n)\ w_2(n)\ \ldots\ w_M(n)]^{\mathrm{T}}$ denotes the additive white noise at the nth snapshot, which is assumed to be independent with transmitted sources. $\mathbf{A} = [\mathbf{a}(\theta_1)\ \mathbf{a}(\theta_2)\ \cdots\ \mathbf{a}(\theta_K)]$ denotes the steering matrix, $\mathbf{a}(\theta_k) = [a_1(\theta_k)\ a_2(\theta_k)\ \cdots\ a_M(\theta_k)]^{\mathrm{T}}$ with $a_m(\theta_k) = \exp(-\mathrm{j}(2\pi\xi_m \sin\theta_k/\lambda))$ denotes the steering vector of the kth source, and λ denotes the source wavelength.

Thus, the covariance matrix of array output can be expressed and calculated as

$$\begin{aligned}\mathbf{R} &= E\left(\mathbf{x}(n)\mathbf{x}^{\mathrm{H}}(n)\right) \\ &= \mathbf{A}\mathrm{diag}\left(\left[\,\sigma_1^2\ \sigma_2^2\ \cdots\ \sigma_K^2\,\right]^{\mathrm{T}}\right)\mathbf{A}^{\mathrm{H}} + \sigma_{\mathrm{w}}^2\mathbf{I}_M \\ &\approx \frac{1}{N}\sum_{n=1}^{N}\mathbf{x}(n)\mathbf{x}^{\mathrm{H}}(n) \end{aligned} \tag{3}$$

where $(\bullet)^{\mathrm{H}}$ denotes Hermitian transpose operator, σ_k^2 and σ_{w}^2 respectively denote the power of the kth source and that of white noise, $\mathbf{I}_M$ denotes M dimensional identity matrix.

III. Reduced Dimension With Atomic Norm

Since the covariance matrix as a constraint for solving optimization problem [7] requires high computational cost, the eigendecomposition is exploited to construct a measurement vector in the form of atomic norm. The atomic norm is the minimum number of "atoms" to reconstruct the measurement vector, thus the gridless DOA is the continuous analog to the gridded compressive DOA.

Consider the eigendecomposition of covariance matrix with multiple snapshots expressed as

$$\mathbf{R} = \mathbf{U}_{\mathbf{S}}\mathbf{\Delta}_{\mathbf{S}}\mathbf{U}_{\mathbf{S}}^{\mathrm{H}} + \mathbf{U}_{\mathbf{W}}\mathbf{\Delta}_{\mathbf{W}}\mathbf{U}_{\mathbf{W}}^{\mathrm{H}} \tag{4}$$

where $\mathbf{\Delta}_{\mathbf{S}}$ and $\mathbf{\Delta}_{\mathbf{W}}$ respectively denote the diagonal matrix with K larger eigenvalues and that with the remaining M-K smaller eigenvalues, $\mathbf{U}_{\mathbf{S}}$ and $\mathbf{U}_{\mathbf{W}}$ respectively denote $M\times K$ dimensional signal subspace and $M\times(M\text{-}K)$ dimensional noise subspace. Due to the orthogonality of signal subspace and noise subspace, the multiplication of covariance and signal subspace can be rewritten as

$$\mathbf{R}\mathbf{U}_{\mathbf{S}} = \mathbf{U}_{\mathbf{S}}\mathbf{\Delta}_{\mathbf{S}}\mathbf{U}_{\mathbf{S}}^{\mathrm{H}}\mathbf{U}_{\mathbf{S}} + \mathbf{U}_{\mathbf{W}}\mathbf{\Delta}_{\mathbf{W}}\mathbf{U}_{\mathbf{W}}^{\mathrm{H}}\mathbf{U}_{\mathbf{S}} = \mathbf{U}_{\mathbf{S}}\mathbf{\Delta}_{\mathbf{S}}. \tag{5}$$

In addition, by multiplying $\mathbf{U}_{\mathbf{S}}$ on both sides of (3), we can obtian

$$\mathbf{R}\mathbf{U}_{\mathbf{S}} = \mathbf{A}\mathbf{\Delta}_{\mathbf{S}}\mathbf{A}^{\mathrm{H}}\mathbf{U}_{\mathbf{S}} + \sigma_{\mathrm{w}}^2\mathbf{I}_M\mathbf{U}_{\mathbf{S}}. \tag{6}$$

Then, by combining (5) and (6), we can further obtian

$$\mathbf{A}\mathbf{\Delta}_{\mathbf{S}}\mathbf{A}^{\mathrm{H}}\mathbf{U}_{\mathbf{S}} = \mathbf{U}_{\mathbf{S}}\mathbf{\Delta}_{\mathbf{S}} - \sigma_{\mathrm{w}}^2\mathbf{I}_M\mathbf{U}_{\mathbf{S}} = \mathbf{U}_{\mathbf{S}}(\mathbf{\Delta}_{\mathbf{S}} - \sigma_{\mathrm{w}}^2\mathbf{I}_M). \tag{7}$$

Herein, by expressing $\mathbf{\Delta}_{\mathbf{S}}\mathbf{A}^{\mathrm{H}}\mathbf{U}_{\mathbf{S}}$ as $\mathbf{B}$, the left side of (7) can be rewritten as

$$\begin{aligned}&\mathbf{A}\mathbf{\Delta}_{\mathbf{S}}\mathbf{A}^{\mathrm{H}}\mathbf{U}_{\mathbf{S}} = \mathbf{A}\mathbf{B} \\ &= \begin{bmatrix} \sum_{k=1}^{K} a_{1,k}b_{k,1} & \cdots & \sum_{k=1}^{K} a_{1,k}b_{k,p} & \cdots & \sum_{k=1}^{K} a_{1,k}b_{k,K} \\ \vdots & \ddots & \vdots & \ddots & \vdots \\ \sum_{k=1}^{K} a_{M,k}b_{k,1} & \cdots & \sum_{k=1}^{K} a_{M,k}b_{k,p} & \cdots & \sum_{k=1}^{K} a_{M,k}b_{k,K} \end{bmatrix}\end{aligned} \tag{8}$$

for $p = 12,\ldots,K$, where $b_{k,p}$ denotes the element of the kth row at the qth column of $\mathbf{B}$.

Moreover, the right side of (7) can be rewritten as

$$\begin{aligned}&\mathbf{U}_{\mathbf{S}}(\mathbf{\Delta}_{\mathbf{S}} - \sigma_{\mathrm{w}}^2\mathbf{I}_M) \\ &= \begin{bmatrix} \mu_{1,1}(\sigma_1^2-\sigma_{\mathrm{w}}^2) & \cdots & \mu_{1,p}(\sigma_p^2-\sigma_{\mathrm{w}}^2) & \cdots & \mu_{1,K}(\sigma_K^2-\sigma_{\mathrm{w}}^2) \\ \vdots & \ddots & \vdots & \ddots & \vdots \\ \mu_{M,1}(\sigma_1^2-\sigma_{\mathrm{w}}^2) & \cdots & \mu_{M,p}(\sigma_p^2-\sigma_{\mathrm{w}}^2) & \cdots & \mu_{M,K}(\sigma_K^2-\sigma_{\mathrm{w}}^2) \end{bmatrix}\end{aligned} \tag{9}$$

where $\mu_{m,p}$ denotes the element of the mth row at the pth column in $\mathbf{U}_{\mathbf{S}}$. Thus, by combining (8) and (9), $\mu_{m,p}$ can be calculated as

$$\mu_{m,p} = \frac{1}{\sigma_p^2 - \sigma_{\mathrm{w}}^2}\sum_{k=1}^{K} a_{m,k}b_{k,p}\,. \tag{10}$$

Adding up $\mu_{m,p}$ multiplied by the corresponding eigenvalue σ_p^2, we can obtain

$$\begin{aligned}\sum_{p=1}^{K}\sigma_p^2\mu_{m,p} &= \sum_{p=1}^{K}\frac{\sigma_p^2}{\sigma_p^2-\sigma_{\mathrm{w}}^2}\sum_{k=1}^{K}a_{m,k}b_{k,p} \\ &= \sum_{k=1}^{K}a_{m,k}\sum_{p=1}^{K}\frac{\sigma_p^2}{\sigma_p^2-\sigma_{\mathrm{w}}^2}b_{k,p}\end{aligned} \tag{11}$$

By defining $\sum_{p=1}^{K}(\sigma_p^2 b_{k,p})/(\sigma_p^2-\sigma_{\mathrm{w}}^2)$ as f_k, we can obtain

$$\mathbf{y} = \sum_{p=1}^{K}\sigma_p^2\boldsymbol{\mu}_p = \sum_{k=1}^{K} f_k\mathbf{a}(\theta_k) \tag{12}$$

where $\boldsymbol{\mu}_p = [\mu_{1,p}, \mu_{2,p}, \ldots, \mu_{M,p}]^{\mathrm{T}}$ denotes the pth eigenvector corresponding to the pth eigenvalue σ_p^2 of covariance matrix. Considering that f_k can be expressed as $|f_k|\exp(\mathrm{j}\varphi_k)$, the measurement vector $\mathbf{y}$ can be rewritten as (13) shown at the bottom of the next page, where $|\,\bullet\,|$ denotes the absolute value, $|f_k|$ and φ_k respectively denote the amplitude and phase of f_k. The atomic set can be expressed as

$$\mathcal{A} = \left\{\exp(j\varphi)\mathbf{a}(\theta)\,\middle|\,\varphi\in[0,2\pi), \theta\in[-\frac{\pi}{2},\frac{\pi}{2}]\right\} \tag{14}$$

where $\mathbf{a}(\theta) = [a_1(\theta)\ a_2(\theta)\ \cdots\ a_M(\theta)]^{\mathrm{T}}$. Thus, exploiting the linear combination [8], the atomic ℓ_0 norm of the measurement vector $\mathbf{y}$ is given by

$$\|\mathbf{y}\|_{\mathcal{A},0} = \inf_{\substack{|f_k|\geq 0 \\ \exp(j\varphi_k)\mathbf{a}(\theta_k)\in\mathcal{A}}}\left\{K : \mathbf{y} = \sum_{k=1}^{K}|f_k|\exp(j\varphi_k)\mathbf{a}(\theta_k)\right\}. \tag{15}$$

Authorized licensed use limited to: Chang'an University. Downloaded on December 05,2022 at 14:08:01 UTC from IEEE Xplore. Restrictions apply.

IV. Deep Alternating Projection Network

Considering the model-based alternating projection method [9] requires a certain number of iterations, we apply the deep unfolding network to accelerate convergence rate. As shown in Fig. 2, the deep alternating projection network is proposed and trained to achieve gridless DOA estimation, where the iterations of alternating projection algorithm are corresponding to the layers of network. Herein, the projection onto positive semi-definite (PSD) set in the *l*th layer can be expressed as

$$\mathbf{\Lambda}^{(l)}=P_D(\mathbf{Z}^{(l-1)}) = \sum_{m=1}^{M} \max\left(0, \eta_m^{(l-1)}\right) \boldsymbol{\psi}_m^{(l-1)} \left(\boldsymbol{\psi}_m^{(l-1)}\right)^{\mathrm{H}} \tag{16}$$

for $l = 12, \ldots, L$, $\eta_m^{(l-1)}$ and $\boldsymbol{\psi}_m^{(l-1)}$ respectively denote the *m*th eigenvalue and the corresponding eigenvector of $\mathbf{Z}^{(l-1)}$, the input of the first layer $\mathbf{Z}^{(0)}$ is give by

$$\mathbf{Z}^{(0)} = \begin{bmatrix} \mathbf{R} & \mathbf{y} \\ \mathbf{y}^{\mathrm{H}} & \mathbf{y}^{\mathrm{H}}\mathbf{y} \end{bmatrix}. \tag{17}$$

Different from the Hermitian Toeplitz set of uniform linear array, the projection onto irregular Hermitian Toeplitz set of nested array is defined as

$$\mathbf{\Omega}^{(l)}=P_H(\mathbf{\Lambda}^{(l-1)}), \tag{18}$$

where the (τ_1, τ_2)th element of $\mathbf{\Omega}^{(l)}$ can be calculated as

$$\mathbf{\Omega}^{(l)}_{\tau_1,\tau_2} = \begin{cases} \text{mean}\left(\mathbf{\Lambda}^{(l-1)}_{\tau_3,\tau_4} + \left(\mathbf{\Lambda}^{(l-1)}_{\tau_4,\tau_3}\right)^*\right) \tau_1 \le \tau_2 \\ \text{mean}\left(\left(\mathbf{\Lambda}^{(l-1)}_{\tau_3,\tau_4}\right)^* + \mathbf{\Lambda}^{(l-1)}_{\tau_4,\tau_3}\right) \tau_1 > \tau_2 \end{cases} \tag{19}$$

$(\bullet)^*$denotes complex conjugate operator, $\tau_1, \tau_2 \le M$, $\xi_{\tau_1} - \xi_{\tau_2}=\xi_{\tau_3} - \xi_{\tau_4}$. Thus, $\mathbf{Z}^{(l)}$ is updated as

$$\mathbf{Z}^{(l)} = \begin{bmatrix} \mathbf{\Omega}^{(l)} & \mathbf{y} \\ \mathbf{y}^{\mathrm{H}} & \mathbf{\Lambda}^{(l)}_{M+1,M+1} \end{bmatrix}. \tag{20}$$

By replacing the non-convex optimization problem with its convex analog, the loss function of the network is given by

$$\min \mathrm{tr}(\mathbf{Z}^{(L)}) \tag{21}$$

where tr(.) denotes the trace of matrix. In practice, by exploiting the irregular Vandermonde decomposition and irregular root-MUSIC method in [9] with the output of the *L*th layer $\mathbf{\Omega}^{(L)}$, the gridless DOA via nested array can be estimated as

$$\min \left(\sum_{m_1=1}^{M} \sum_{m_2=1}^{M} \hat{\mathbf{V}}_{m_1,m_2} \gamma^{\xi_{m_1}-\xi_{m_2}} \right) \text{s.t.} |\gamma| = 1 \tag{22}$$

$$\hat{\theta} = -\arcsin(\angle\gamma/\pi) \tag{23}$$

where $\hat{\mathbf{V}}_{m_1,m_2}$ denotes the (m_1, m_2)th element of $\hat{\mathbf{U}}_{\mathbf{W}}\hat{\mathbf{U}}_{\mathbf{W}}^{\mathrm{H}}$, $\hat{\mathbf{U}}_{\mathbf{W}}$ denotes the noise subspace of $\mathbf{\Omega}^{(L)}$.

V. Simulation Experiments

In this section, we exploit the simulation experiments to demonstrate the effectiveness and performance of the proposed networks for gridless DOA estimation with nested array, where the locations of sensors are set as [1]–[5], [10], [15],[20]]*d*. Herein, the layer number of the proposed network is set as 6, the training dataset is generated by two sources, where the gridless DOAs are selected from $-60°$ to 60°, the SNR is selected from 0dB to 20dB, the snapshot number is selected from 50 to 300. In the training progress, the training samples are randomly divided into 80% for training and 20% for validation, the mini-batch size, epoch and learning rate are respectively set to 16, 16 and 0.01.

TABLE I
The Estimates of Gridless DOAs

Source number	Setting values of gridless DOAs	DOAs estimates of proposed network	DOAs estimates of original algorithm
1	-10.1	-10.099	-10.105
2	-10.1, 0.3	-10.101, 0.297	-10.107, 0.295
3	-10.1, 0.3, 2.5	-10.100, 0.302, 2.498	-10.095, 0.294, 2.495

A. Effectiveness and Generalization Ability

In this subsection, we first apply the output of network and irregular root-MUSIC method to verify the effectiveness of the proposed network, where the estimates of gridless DOAs are shown in Table I.

It can be noticed that the proposed network can achieve gridless DOA estimation for different number of sources, which demonstrates that the generalization ability of the proposed network. As depicted in Fig. 3, the effectiveness can also be verified by the irregular null spectrum from (22), where *x*-axis and *y*-axis in Fig. 3(a) respectively denote the real part and imaginary part of γ, and the blue curve in Fig. 3(b) denotes the corresponding magnitude of the unit circle in global graph.

B. Computational Complexity and Convergence Rate

Generally, the computational complexity of deep unfolding network is proportional to the number of layers. As for the computational complexity of each layer, the calculation of eigen-decomposition for the projection onto positive semi- definite set in (16) is $\mathcal{O}((M+1)^3)$, that of the projection onto irregular Hermitian Toeplitz set in (18) is $\mathcal{O}(M)$. Compared with the reduced dimension of measurement vector in the proposed network, the original alternating projection method with covariance matrix in [9] requires $\mathcal{O}((M+N)^3)$ for the projection onto positive semi-definite set. Besides, we compare the computational complexity of the proposed networks with the off-grid sparse Bayesian learning (SBL) method in [6] and the gridless atomic norm minimization (ANM) method in [10]. As for off-grid SBL method, the calculation of each iteration is $\mathcal{O}(QM^4)$, where Q denotes the number of grid points. As for the ANM method, the calculation of covariance matrix requires M^2N multiplications and $M^2(N-1)$ additions, the SDP problem is solved by the CVX toolbox. Further, we compare the average computational time of 100 Monte-Carlo trials under the environment of Intel i5-337U CPU, where the time cost of the proposed network, original

$$\mathbf{y} = \left[\sum_{k=1}^{K} |f_k| \exp(\mathrm{j}\varphi_k) a_1(\theta_k) \sum_{k=1}^{K} |f_k| \exp(\mathrm{j}\varphi_k) a_2(\theta_k) \cdots \sum_{k=1}^{K} |f_k| \exp(\mathrm{j}\varphi_k) a_M(\theta_k) \right]^{\mathrm{T}} \tag{13}$$

Authorized licensed use limited to: Chang'an University. Downloaded on December 05,2022 at 14:08:01 UTC from IEEE Xplore. Restrictions apply.

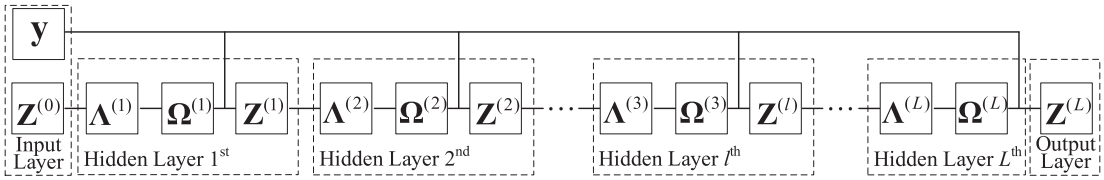

Fig. 2. The structure of deep alternating projection network.

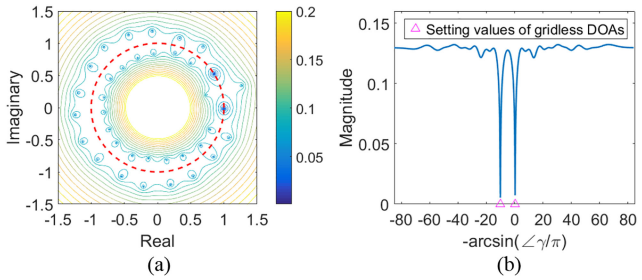

Fig. 3. Irregular null spectrum. (a) Global graph. (b) Evaluation on unit circle.

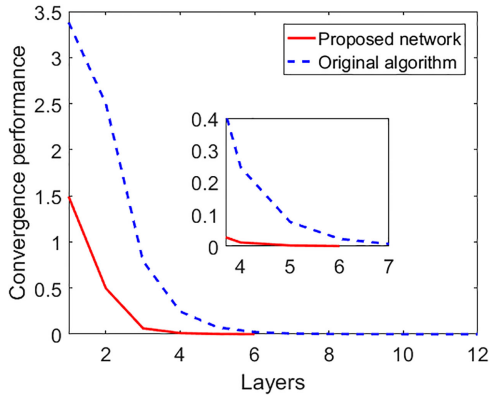

Fig. 4. Comparsion of convergence performance.

AP method, off-grid SBL method and ANM method is 0.35s, 2.68s, 0.85s and 1.27s, respectively. We can demonstrate that the proposed network with can significantly reduce computational complexity.

Moreover, when the gridless DOAs of the testing data are set as $-10.1°$ and $0.3°$, the comparsion of convergence rate is depicted in Fig. 4, which is defined as

$$\frac{\left\|\mathbf{\Omega}^{(l)}-\mathbf{\Omega}^{(l-1)}\right\|_2}{\left\|\mathbf{\Omega}^{(l-1)}\right\|_2} \tag{24}$$

where $\|\bullet\|_2$ denotes ℓ_2 norm. It can be noticed that the convergence of the trained network requires 5 layers and that of the original alternating algorithm requires 8 layers, which demonstrates that the trained network can accelerate the convergence speed and reduce computational complexity.

C. Comparison of RMSE

In this subsection, we perform the root mean square error (RMSE) of Monte-Carlo simulation experiments to investigate the performance of the proposed networks in comparison with

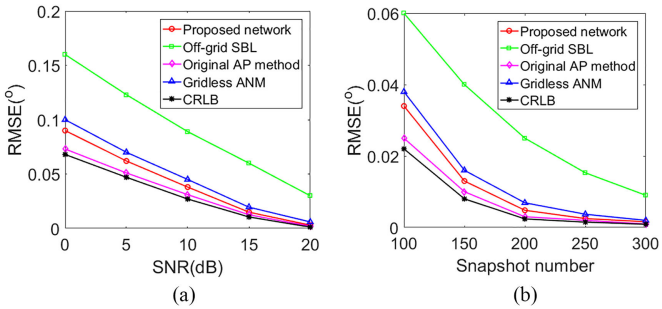

Fig. 5 RMSEs of gridless DOA estimation. (a) SNR. (b) Snapshot.

the off-grid SBL method in [6], the original alternating projection (AP) method in [9], the gridless ANM in [10] and Cramér-Rao Lower Bound (CRLB). Herein, the RMSE of gridless DOA estimation is defined as

$$\sqrt{\frac{1}{VK}\sum_{v=1}^{V}\sum_{k=1}^{K}\left(\hat{\theta}_k^{(v)}-\theta_k\right)^2} \tag{25}$$

where K and V respectively denote the number of sources and Monte-Carlo simulation experiments, θ_k denotes the real DOA of the kth source, $\hat{\theta}_k^{(v)}$ denotes the estimated DOA of the kth source in the vth Monte-Carlo simulation experiment.

Herein, we execute 300 Monte-Carlo simulation experiments and the RMSE of gridless DOA estimation is displayed in Fig. 5, where the DOAs are respectively set to $-10.1°$ and $0.3°$. It can be noticed that the RMSE decreases with the increase of SNR and snapshot. Besides, it can be noticed that the accuracy of the proposed network is higher than that of the off-grid SBL method and gridless ANM method. Due to the additional error caused by calculating the measurement vector in (12), the accuracy of the proposed network is lower than that of original alternating projection method with covariance matrix.

VI. Conclusion

In this letter, we present a deep alternating projection network to achieve gridless DOA estimation with nested array. In order to reduce the computational cost during the progress of projection, the covariance matrix is transformed into a measurement vector in the form of atomic norm. Then, the proposed network is trained to alternately obtain the positive semi-definite matrix and the corresponding irregular Hermitian Toeplitz matrix of nested array, where the loss function is related to the trace of network output. Finally, the irregular root-MUSIC method is applied to obtain gridless DOA. Simulation results demonstrate that the proposed network can accelerate the convergence speed and reduce computational complexity.

Authorized licensed use limited to: Chang'an University. Downloaded on December 05,2022 at 14:08:01 UTC from IEEE Xplore. Restrictions apply.

REFERENCES

[1] J. Shi, F. Wen, and T. Liu, "Nested MIMO radar: Coarrays, tensor modeling, and angle estimation," *IEEE Trans. Aerosp. Electron. Syst.*, vol. 57, no. 1, pp. 573–585, Feb. 2021.

[2] J. Shi, Z. Yang, and Y. Liu, "On parameter identifiability of diversity-smoothing-based MIMO radar," *IEEE Trans. Aerosp. Electron. Syst.*, vol. 58, no. 3, pp. 1660–1675, Jun. 2022.

[3] J. Li, P. Li, P. Li, L. Tang, X. Zhang, and Q. Wu, "Self-position awareness based on cascade direct localization over multiple source data," *IEEE Trans. Intell. Transp. Syst.*, early access, May 2, 2022, doi: 10.1109/TITS.2022.3170465.

[4] H. Huang, J. Yang, H. Huang, Y. Song, and G. Gui, "Deep learning for super-resolution channel estimation and DOA estimation based massive MIMO system," *IEEE Trans. Veh. Technol.*, vol. 67, no. 9, pp. 8549–8560, Sep. 2018.

[5] C. Zhou, Y. Gu, Z. Shi, and Y. D. Zhang, "Off-grid direction-of-arrival estimation using coprime array interpolation," *IEEE Signal Process. Lett.*, vol. 25, no. 11, pp. 1710–1714, Nov. 2018.

[6] F. Chen, J. Dai, N. Hu, and Z. Ye, "Sparse Bayesian learning for off-grid DOA estimation with nested arrays," *Digit. Signal Process.*, vol. 82, pp. 187–193, 2018.

[7] Z. Yang and L. Xie, "On gridless sparse methods for line spectral estimation from complete and incomplete data," *IEEE Trans. Signal Process.*, vol. 63, no. 12, pp. 3139–3153, Jun. 2015.

[8] T. Chen, L. Shi, and M. Shen, "Gridless DOA estimation algorithm based on M-FIPM," *Syst. Eng. Electron.*, vol. 44, no. 2, pp. 427–433, 2022.

[9] M. Wagner, Y. Park, and P. Gerstoft, "Gridless DOA estimation and root-MUSIC for non-uniform linear arrays," *IEEE Trans. Signal Process.*, vol. 69, pp. 2144–2157, 2021.

[10] T. Chen, L. Shi, and L. Guo, "Gridless direction of arrival estimation exploiting sparse linear array," *IEEE Signal Process. Lett.*, vol. 27, pp. 1625–1629, 2020.

[11] P. Pal and P. P. Vaidyanathan, "Nested arrays: A novel approach to array processing with enhanced degrees of freedom," *IEEE Trans. Signal Process.*, vol. 58, no. 8. pp. 4167–4181, Aug. 2010.

[12] H. Zheng, Z. Shi, C. Zhou, M. Haardt, and J. Chen, "Coupled coarray tensor CPD for DOA estimation with coprime L-shaped array," *IEEE Signal Process. Lett.*, vol. 28, pp. 1545–1549, 2021.

[13] C. Zhou, Y. Gu, X. Fan, Z. Shi, G. Mao, and Y. D. Zhang, "Direction-of-arrival estimation for coprime array via virtual array interpolation," *IEEE Trans. Signal Process.*, vol. 66, no. 22, pp. 5956–5971, Nov. 2018.

[14] V. Monga, Y. Li, and Y. C. Eldar, "Algorithm unrolling: Interpretable, efficient deep learning for signal and image processing," *IEEE Signal Process. Mag.*, vol. 38, no. 2, pp. 18–44, Mar. 2021.

[15] K. Gregor and Y. LeCun, "Learning fast approximations of sparse coding," in *Proc. Int. Conf. Mach. Learn.*, 2010, pp. 399–406.

[16] M. Borgerding, P. Schniter, and S. Rangan, "AMP-inspired deep networks for sparse linear inverse problems," *IEEE Trans. Signal Process.*, vol. 65, no. 16, pp. 4293–4308, Aug. 2017.

[17] Y. Yang, J. Sun, H. Li, and Z. Xu, "Deep ADMM-Net for compressive sensing MRI," in *Proc. 30th Conf. Neural Inf. Process. Syst.*, 2016, pp. 10–18.

[18] S. A. H. Hosseini, B. Yaman, S. Moeller, M. Hong, and M. Akçakaya, "Dense recurrent neural networks for accelerated MRI: History-cognizant unrolling of optimization algorithms," *IEEE J. Sel. Top. Signal Process.*, vol. 14, no. 6, pp. 1280–1291, Oct. 2020.

[19] R. Li, S. Zhang, C. Zhang, Y. Liu, and X. Li, "Deep learning approach for sparse aperture ISAR imaging and autofocusing based on complex-valued ADMM-net," *IEEE Sensors J.*, vol. 21, no. 3, pp. 3437–3451, Feb. 2021.

Authorized licensed use limited to: Chang'an University. Downloaded on December 05,2022 at 14:08:01 UTC from IEEE Xplore. Restrictions apply.